Article ID: 1671-3664(2004)02-0249-14

Diffraction of anti-plane SH waves by a semi-circular cylindrical hill with an inside concentric semi-circular tunnel

Vincent W. Lee[1†], Luo Hao (罗 昊)[2,3‡] and Liang Jianwen (梁建文)[3†]

1. *Dept. of Civil and Environmental Engineering, Univ. of Southern California, Los Angeles, CA 90089-2531, USA*
2. *Civil Engineering and Architecture Experiment Center, Dept. of Civil Engineering, Shanghai Jiaotong Univ., 800 Dongchuan Rd., Shanghai 200240, China*
3. *Dept. of Civil Engineering, Tianjin Univ., Tianjin 300072, China*

Abstract: A closed-form analytic solution of two-dimensional scattering and diffraction of plane SH waves by a semi-cylindrical hill with a semi-cylindrical concentric tunnel inside an elastic half-space is presented using the cylindrical wave functions expansion method. The solution is reduced to solving a set of infinite linear algebraic equations. Fourier expansion theorem with the form of complex exponential function and cosine function is used. Numerical solutions are obtained by truncation of the infinite equations. The accuracy of the presented numerical results is carefully verified.

Keywords: SH waves; hill; tunnels; close-form analytic solution; amplifications.

I Introduction

One of the most important problems in earthquake engineering and seismology is to explain the amplification or deamplification effects to earthquake responses by surface and subsurface topography. Due to the difficulties in formulating the solutions, very limit analytical solutions are hitherto available: semi-cylindrical alluvial valley (Trifunac, 1971), semi-elliptical alluvial valley (Wong and Trifunac, 1974), circular underground cavity (Lee, 1977), semi-cylindrical hill (Yuan and Men, 1992), and cylindrical hill of circular-arc cross-section (Yuan and Liao, 1996). Furthermore, most of the analytical solutions focus on certain topography, such as a canyon, valley, hill or cavity, etc. The interaction between topography and substructure, such as between a tunnel or cavity, is not as frequently studied. Diffraction from a canyon above a subsurface unlined tunnel (Lee *et al.*, 1999) and multiple foundations above a subway (Lee and Chen, 1998) have been examined. Hilly topography is also a common local surface irregularity. In reality, a mountain tunnel is very common. It is necessary to consider the influence from the site effect when tunnels or pipes are constructed through mountains in seismic areas. Again, cavities are ordinary in a mountainous area, especially in the karst region.

In this paper, a closed-form analytic solution of two-dimensional scattering of plane SH waves by a semi-circular cylindrical hill with a semi-circular concentric tunnel inside on a half-space is presented using the wave functions expansion method. The solution is reduced to solving a set of infinite linear algebraic equations. Unlike the former paper (Yuan and Men, 1992), Fourier expansion theorem with the form of both the complex exponential function and cosine function are used. Numerical solutions are obtained by truncation of the infinite equations and singular value decomposition method. The efficiency of the computer program is improved distinctly by using the Fourier expansion theorem algorithm with the form of complex exponential function as opposed to the sines and cosines trigonometric function. The accuracies of the numerical results are checked by the convergence of the ground surface displacement and residual errors of boundary conditions by increasing the truncation order. The effects of the frequencies, incident angles of the incident waves and the radius of the tunnel on displacement amplitude of ground surface are illustrated. It was shown that the existence of a hill and tunnel has a significant effect on the ground surface motion nearby.

2 Mathematical model

The cross section of the two-dimensional model studied in this paper is shown in Fig. 1. It represents an elastic, isotropic and homogeneous half-space with a

Correspondence to: Vincent W. Lee, Dept. of Civil and Environmental Engineering, Univ. of Southern California, Los Angeles, CA 90089-2531, USA
Tel: 213-740-0568; Fax: 213-744-1426
E-mail: vlee@usc.edu
†Professor; ‡Assistant Engineer
Received date: 2004-06-08; **Accepted date**: 2004-08-30

semi-cylindrical hill of radius a. There is a semi-circular concentric tunnel inside the hill. The free surface of the half-space consists of a flat surface Γ and semi-circular hilly boundary L. The upper and flat ground boundary of the semi-circular tunnel are marked as L_1 and Γ_1 respectively. The radius of the tunnel is a_1. The height and half-width of the hill is h and b. For the semi-cylindrical hill, $b=h$.

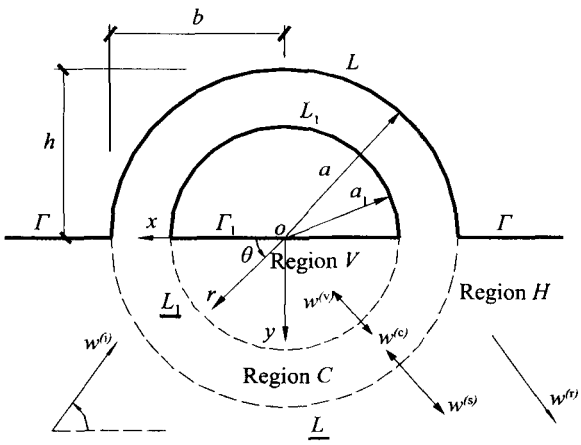

Fig. 1 Mathematical model

For the convenience of using wave functions for the solution, the half-space can be divided into three parts as shown in Fig. 2. The first one is the annular region C including the hill, whose outer upper and lower boundary are L and $\underline{L}$ respectively, and the inner upper and lower boundary are L_1 and $\underline{L}_1$. The second region is the half-space canyon H, which has a common boundary $\underline{L}$ with region C and a flat ground surface boundary Γ. The last region is the semi-circular region V, the semi-circular "valley" region bounded by Γ_1 and $\underline{L}_1$. The original model is thus divided into three individual regions and a Fourier-Bessel wave function expansion is used in each of these regions. The boundary conditions are: the traction-free boundary conditions on L in region C; the traction-free boundary conditions on Γ in region H; the traction-free boundary conditions on Γ_1 in region V; displacement and stress continuity boundary conditions on $\underline{L}$ between region C and H; and displacement and stress continuity boundary conditions on $\underline{L}_1$ between region C and V. Note that there are two different boundary conditions on the full circular boundary such as $L+\underline{L}$ and $L_1+\underline{L}_1$. Therefore, this model is a mixed boundary problem.

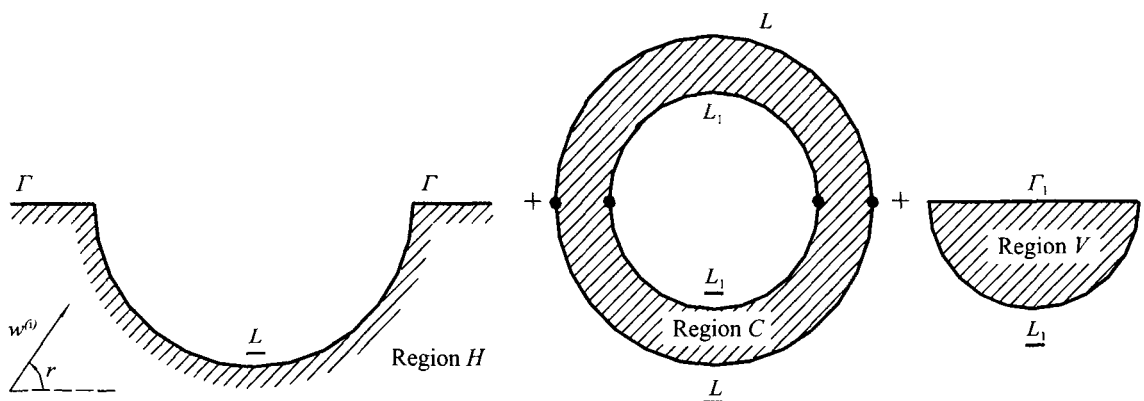

Fig. 2 Division of the half-space

3 Incident and scattered waves: Fourier-Bessel series expansion

The excitation of the half-space consists of a steady-state set of incident plane SH waves, with an angle of incidence γ and particle motions in the z-directions (anti-plane). It can be represented in the Cartesian coordinate system with origin in O by

$$w^{(i)} = w_0 \cdot \exp\left[-\mathrm{i}\omega\left(t + x/c_x + y/c_y\right)\right] \tag{1}$$

where $\mathrm{i} = \sqrt{-1}$ means the imaginary unit, c_x and c_y are the phase velocities along the x-direction and y-direction, respectively. ω and w_0 are the circular frequency and amplitude of the waves. In Eq. (1), the time factor $\exp(-\mathrm{i}\omega t)$ is omitted, similarly hereinafter.

The displacement in the half-space region H can be expressed by

$$w = w^{(\mathrm{ff})} + w^{(\mathrm{s})} \tag{2}$$

where $w^{(\mathrm{ff})}$ represents the free field displacement in the half-space; and $w^{(\mathrm{s})}$ represents the scattering displacement resulting from the interaction between the half-space and boundary $\underline{L}$.

The total displacement field w must satisfy the steady-state elastic wave equation (Helmholtz equation) (Pao and Mow, 1973)

$$\frac{\partial^2 w}{\partial r^2} + \frac{1}{r}\cdot\frac{\partial w}{\partial r} + \frac{1}{r^2}\cdot\frac{\partial^2 w}{\partial \theta^2} = \frac{1}{c_\beta{}^2}\cdot\frac{\partial^2 w}{\partial t^2} \tag{3}$$

and the traction-free boundary conditions

$$\tau_{\theta z}|_{\theta=0,\pi}=0 \qquad \text{at } (r,\theta)\in \Gamma \tag{4}$$

$$\tau_{\theta z}|_{\theta=0,\pi}=0 \qquad \text{at } (r,\theta)\in \Gamma_1 \tag{5}$$

$$\tau_{rz}|_{r=a_1}=0 \qquad \text{at } (r,\theta)\in L \tag{6}$$

$$\tau_{rz}|_{r=a_2}=0 \qquad \text{at } (r,\theta)\in L_1 \tag{7}$$

where the hoop stress $\tau_{\theta z}$ and the radial stress τ_{rz} are given by

$$\tau_{\theta z}=\frac{\mu}{r}\frac{\partial w}{\partial \theta} \tag{8}$$

$$\tau_{rz}=\mu\frac{\partial w}{\partial r} \tag{9}$$

where μ is the shear modulus.

The free field displacement $w^{(\mathrm{ff})}$ consists of the incident wave, $w^{(\mathrm{i})}$ and its reflected wave $w^{(\mathrm{r})}$ on the flat ground surface

$$w^{(\mathrm{ff})}=w^{(\mathrm{i})}+w^{(\mathrm{r})} \tag{10}$$

$w^{(\mathrm{i})}$ is given by Eq. (1), and the reflected plane SH wave $w^{(\mathrm{r})}$ is given by

$$w^{(\mathrm{r})}=w_0\exp\left[-\mathrm{i}\omega(t+x/c_x-y/c_y)\right] \tag{11}$$

Substitute $c_x=c_\beta/\cos\gamma$ and $c_y=c_\beta/\sin\gamma$ into Eqs. (1) and (11), in which c_β is the velocity of the incident SH wave.

$$\begin{cases} w^{(\mathrm{i})}=w_0\exp\left[-\mathrm{i}k(x\cos\gamma+y\sin\gamma)\right] \\ w^{(\mathrm{r})}=w_0\exp\left[-\mathrm{i}k(x\cos\gamma-y\sin\gamma)\right] \end{cases} \tag{12}$$

in which $k=\omega/c_\beta$ is the wave number.

By $x=r\cos\theta$, $y=r\sin\theta$ and the expansion theorem (Abramowitz and Stegun, 1972)

$$\exp(\pm\mathrm{i}kr\cos\theta)=\sum_{n=0}^{\infty}\varepsilon_n(\pm\mathrm{i})^n\mathrm{J}_n(kr)\cos n\theta \tag{13}$$

the free field displacement in the polar coordinate system (r,θ) can be written as

$$w^{(\mathrm{ff})}(r,\theta)=w_0\sum_{n=0}^{\infty}a_{0,n}\mathrm{J}_n(kr)\cos n\theta \tag{14}$$

where $\mathrm{J}_n(\cdot)$ is the Bessel function of the first kind with order n, and

$$a_{0,n}=2\varepsilon_n(-\mathrm{i})^n\cos n\gamma \tag{15}$$

in which $\varepsilon_0=1$, $\varepsilon_n=2$, for $n=1, 2, 3\cdots$. Inserting Eq. (14) into (9) leads to

$$\tau_{rz}^{(\mathrm{ff})}(r,\theta)=\tau_0\sum_{n=0}^{\infty}a_{0,n}\mathrm{J}_n'(kr)\cos n\theta \tag{16}$$

where $\tau_0=\mu k w_0$, representing the stress amplitude of the free-field waves.

The general solution of Eq. (3) satisfying the zero-stress free-field boundary condition Eq. (4) is

$$w^{(\mathrm{s})}(r,\theta)=w_0\sum_{n=0}^{\infty}A_n\mathrm{H}_n^{(1)}(kr)\cos n\theta \tag{17}$$

which represents the scattering wave $w^{(\mathrm{s})}$ resulting from $\underline{L}$. A_n, $n=0, 1, 2, \cdots$ is complex coefficient to be determined and $\mathrm{H}_n^{(1)}(\cdot)$ is the Hankel function of the first kind with order n.

Inserting Eq. (17) into Eq. (8), the stress on the ground surface can be expressed as

$$\tau_{\theta z}^{(\mathrm{s})}(r,\theta)=-\frac{n\mu w_0}{r}\sum_{n=0}^{\infty}A_n\mathrm{H}_n^{(1)}(kr)\sin n\theta \tag{18}$$

Apparently, θ is equal to 0 or π on the boundary Γ, resulting in the zero stress boundary condition Eq. (4) satisfied.

Inserting Eq. (17) into Eq. (9) gives

$$\tau_{rz}^{(\mathrm{s})}(r,\theta)=\tau_0\sum_{n=0}^{\infty}A_n\mathrm{H}_n^{(1)'}(kr)\cos n\theta \tag{19}$$

The total displacement in the cylindrical region C resulting from the refracted waves as inward and outward propagating from boundaries $\underline{L}$, L and L_1, $\underline{L_1}$ separately and satisfying Eq. (3) can be represented as

$$w^{(C)}(r,\theta)=w_0\sum_{n=-\infty}^{\infty}\left[B_n^{(1)}\mathrm{H}_n^{(1)}(kr)+B_n^{(2)}\mathrm{H}_n^{(2)}(kr)\right]\mathrm{e}^{\mathrm{i}n\theta} \tag{20}$$

where $B_n^{(1)}$, $B_n^{(2)}$ are respectively the constant coefficients of the outgoing ($H_n^{(1)}$) and incoming ($H_n^{(2)}$) Hankel wave functions, to be determined. Inserting Eq. (20) into Eq. (9) gives

$$\tau_{rz}^{(C)}(r,\theta)=\tau_0\sum_{n=-\infty}^{\infty}\left[B_n^{(1)}\mathrm{H}_n^{(1)'}(kr)+B_n^{(2)}\mathrm{H}_n^{(2)'}(kr)\right]\mathrm{e}^{in\theta} \tag{21}$$

The inward wave $w^{(V)}$ in region V satisfying Eq. (3) and traction-free boundary condition Eq. (5) is given by

$$w^{(V)}(r,\theta)=w_0\sum_{n=0}^{\infty}C_n\mathrm{J}_n(kr)\cos n\theta \tag{22}$$

where C_n are constants to be determined. Inserting Eq. (22) into Eq. (8) leads to

$$\tau_{\theta z}^{(V)}(r,\theta)=-\frac{n\mu w_0}{r}\sum_{n=0}^{\infty}C_n\mathrm{J}_n(kr)\sin n\theta \tag{23}$$

On the flat ground surface Γ_1 of the tunnel, θ is equal to 0 or π. It is easy to realize that the zero stress boundary condition Eq. (5) is satisfied strictly.

Inserting Eq. (22) into Eq. (9) leads to

$$\tau_{rz}^{(V)}(r,\theta)=\tau_0\sum_{n=0}^{\infty}C_n\mathrm{J}_n'(kr)\cos n\theta \tag{24}$$

4 Mixed boundary conditions

All the waves expanded as Fourier-Bessel series in each region are presented. In what follows, the boundary conditions are introduced and the equations derived for the constant coefficients.

4.1 Stress continuity condition on $\underline{L}$ and the traction-free condition on L:

$$\tau_{rz}^{(C)}(r,\theta)=\tau_{rz}^{(\mathrm{ff})}(r,\theta)+\tau_{rz}^{(\mathrm{s})}(r,\theta),\quad (r,\theta)\in\underline{L} \tag{25}$$

$$\tau_{rz}^{(C)}(r,\theta)=0,\quad (r,\theta)\in L \tag{26}$$

Define an auxiliary function, $\Phi_1(\theta)$, at $r=\alpha$:

$$\begin{aligned}\Phi_1(\theta)&=\frac{1}{\tau_0}\tau_{rz}^{(C)}(a,\theta)\\&=\sum_{n=-\infty}^{\infty}\left[B_n^{(1)}\mathrm{H}_n^{(1)'}(ka)+B_n^{(2)}\mathrm{H}_n^{(2)'}(ka)\right]\mathrm{e}^{in\theta}\\&=\begin{cases}0 & ,\ -\pi\le\theta\le 0\\ \dfrac{1}{\tau_0}\left[\tau_{rz}^{(\mathrm{ff})}(a,\theta)+\tau_{rz}^{(\mathrm{s})}(a,\theta)\right] & ,\ 0<\theta\le\pi\end{cases}\\&=\begin{cases}0 & ,\ -\pi\le\theta\le 0\\ \displaystyle\sum_{n=0}^{\infty}\left[a_{0,n}\mathrm{J}_n'(ka)+A_n\mathrm{H}_n^{(1)'}(ka)\right]\cos n\theta & ,\ 0<\theta\le\pi\end{cases}\end{aligned} \tag{27}$$

From Eq. (27), $\Phi_1(\theta)$ has an exponential Fourier series expansion on $\theta\in[-\pi,\pi]$

$$\Phi_1(\theta)=\sum_{n=-\infty}^{\infty}b_n\mathrm{e}^{in\theta} \tag{28}$$

where, $b_n=\dfrac{1}{2\pi}\displaystyle\int_{-\pi}^{\pi}\Phi_1(\theta)\mathrm{e}^{-in\theta}\mathrm{d}\theta$, for $n=0,\pm1,\pm2,\cdots$.

Compare Eq. (28) with Eq. (27), explicitly

$$b_n=B_n^{(1)}\mathrm{H}_n^{(1)'}(ka)+B_n^{(2)}\mathrm{H}_n^{(2)'}(ka) \tag{29}$$

and

$$\begin{aligned}b_n&=\frac{1}{2\pi}\int_{-\pi}^{\pi}\Phi_1(\theta)\mathrm{e}^{-in\theta}\mathrm{d}\theta\\&=\frac{1}{2\pi}\int_0^{\pi}\sum_{m=0}^{\infty}\left[a_{0,m}\mathrm{J}_m'(ka)+A_m\mathrm{H}_m^{(1)'}(ka)\right]\cos m\theta\,\mathrm{e}^{-in\theta}\mathrm{d}\theta\\&=\frac{1}{2}\sum_{m=0}^{\infty}\left[a_{0,m}\mathrm{J}_m'(ka)+A_m\mathrm{H}_m^{(1)'}(ka)\right]\eta_{m,-n}\end{aligned} \tag{30}$$

in which

$$\eta_{m,\pm n}=\frac{1}{\pi}\int_0^{\pi}\cos m\theta\,\mathrm{e}^{\pm in\theta}\mathrm{d}\theta=c(m,n)\pm\mathrm{i}s(m,n)$$

$$(m=0,1,2,\cdots)\ (n=0,1,2,\cdots) \tag{31}$$

with

$$c(m,n)=\frac{1}{\pi}\int_0^{\pi}\cos m\theta\cos n\theta\mathrm{d}\theta=\begin{cases}1, & m=n=0\\ 1/2, & m=|n|\neq 0\\ 0, & m\neq|n|\end{cases} \tag{32}$$

$$s(m,n)=\frac{1}{\pi}\int_0^{\pi}\cos m\theta\sin n\theta\mathrm{d}\theta=\begin{cases}0\\ (m+n \text{ is even})\\ \dfrac{2n}{\pi(n^2-m^2)}\\ (m+n \text{ is odd})\end{cases} \tag{33}$$

Therefore, compare Eq. (29) with Eq. (30), the boundary equation can be written as

$$\begin{aligned}&2\cdot\left[B_n^{(1)}\mathrm{H}_n^{(1)'}(ka)+B_n^{(2)}\mathrm{H}_n^{(2)'}(ka)\right]\\&=\sum_{m=0}^{\infty}\left[a_{0,m}\mathrm{J}_m'(ka)+A_m\mathrm{H}_m^{(1)'}(ka)\right]\eta_{m,-n}\\&\qquad(n=0,\ \pm1,\ \pm2,\cdots)\end{aligned} \tag{34}$$

4.2 Displacement continuity condition on $\underline{L}$:

$$w^{(C)}(r,\theta)=w^{(\mathrm{ff})}(r,\theta)+w^{(\mathrm{s})}(r,\theta),\quad (r,\theta)\in\underline{L} \tag{35}$$

Define an auxiliary function $\Psi_1(\theta)$, for $\theta\in[0,\pi]$:

$$\begin{aligned}\Psi_1(\theta)&=\frac{1}{w_0}w^{(C)}(a,\theta)\\&=\sum_{n=-\infty}^{\infty}\left[B_n^{(1)}\mathrm{H}_n^{(1)}(ka)+B_n^{(2)}\mathrm{H}_n^{(2)}(ka)\right]\mathrm{e}^{in\theta}\\&=\frac{1}{w_0}\left[w^{(\mathrm{ff})}(a,\theta)+w^{(\mathrm{s})}(a,\theta)\right]\\&=\sum_{m=0}^{\infty}\left[a_{0,m}\mathrm{J}_m(ka)+A_m\mathrm{H}_m^{(1)}(ka)\right]\cos m\theta\end{aligned} \tag{36}$$

It is easy to see that $\Psi_1(\theta)$ is (a cosine even) function about θ in the interval $[0,\pi]$. Making $\Psi_1(\theta)$ cosine series Fourier expansion on $\theta\in[0,\pi]$:

$$\Psi_1(\theta)=\sum_{m=0}^{\infty}a_m\cos m\theta \tag{37}$$

with

$$a_m=(\varepsilon_m/\pi)\int_0^{\pi}\Psi_1(\theta)\cos m\theta\mathrm{d}\theta,\varepsilon_0=1,\varepsilon_m=2,m=1,2,3\ldots$$

Compare Eq. (37) with Eq. (36)

$$a_m=a_{0,m}\mathrm{J}_m(ka)+A_m\mathrm{H}_m^{(1)}(ka) \tag{38}$$

and

$$a_m=\varepsilon_m\sum_{n=-\infty}^{\infty}\left[B_n^{(1)}\mathrm{H}_n^{(1)}(ka)+B_n^{(2)}\mathrm{H}_n^{(2)}(ka)\right]\eta_{m,n} \tag{39}$$

with $\eta_{m,n}$ defined earlier in Eq. (31). Hence, compare Eq. (38) with Eq. (39)

$$\begin{aligned}&\varepsilon_m\sum_{n=-\infty}^{\infty}\left[B_n^{(1)}\mathrm{H}_n^{(1)}(ka)+B_n^{(2)}\mathrm{H}_n^{(2)}(ka)\right]\eta_{m,n}\\&=a_{0,m}\mathrm{J}_m(ka)+A_m\mathrm{H}_m^{(1)}(ka)\\&\qquad(m=0,\ 1,\ 2,\cdots)\end{aligned} \tag{40}$$

4.3 Stress continuity condition on $\underline{L_1}$ and traction-free condition on L_1:

$$\tau_{rz}^{(C)}(r,\theta)=\tau_{rz}^{(V)}(r,\theta),\quad (r,\theta)\in\underline{L_1} \tag{41}$$

$$\tau_{rz}^{(C)}(r,\theta)=0,\quad (r,\theta)\in L_1 \tag{42}$$

Define an auxiliary function $\Phi_2(\theta)$, at $r=\alpha_1$:

$$\begin{aligned}\Phi_2(\theta)&=\frac{1}{\tau_0}\tau_{rz}^{(C)}(a_1,\theta)\\&=\sum_{n=-\infty}^{\infty}\left[B_n^{(1)}\mathrm{H}_n^{(1)'}(ka_1)+B_n^{(2)}\mathrm{H}_n^{(2)'}(ka_1)\right]\mathrm{e}^{in\theta}\\&=\begin{cases}0, & -\pi\le\theta\le 0\\ \dfrac{1}{\tau_0}\tau_{rz}^{(V)}(a_1,\theta), & 0<\theta\le\pi\end{cases}\\&=\begin{cases}0, & -\pi\le\theta\le 0\\ \displaystyle\sum_{n=0}^{\infty}C_n\mathrm{J}_n'(ka_1)\cos n\theta, & 0<\theta\le\pi\end{cases}\end{aligned} \tag{43}$$

Similarly, making Eq. (43), $\Phi_2(\theta)$, an exponential Fourier series expansion on $\theta \in [-\pi, \pi]$

$$\Phi_2(\theta) = \sum_{n=-\infty}^{\infty} b_n' e^{in\theta} \tag{44}$$

where, $b_n' = \frac{1}{2\pi}\int_{-\pi}^{\pi} \Phi_2(\theta) e^{-in\theta} d\theta$, for $n = 0, \pm 1, \pm 2, \cdots$.

Compare Eq. (44) with Eq. (43)

$$b_n' = B_n^{(1)} H_n^{(1)'}(ka_1) + B_n^{(2)} H_n^{(2)'}(ka_1) \tag{45}$$

and

$$\begin{aligned} b_n' &= \frac{1}{2\pi}\int_{-\pi}^{\pi} \Phi_2(\theta) e^{-in\theta} d\theta \\ &= \frac{1}{2\pi}\int_0^{\pi} \sum_{m=0}^{\infty} C_m J_m'(ka_1) \cos m\theta \, e^{-in\theta} d\theta \\ &= \frac{1}{2}\sum_{m=0}^{\infty} C_m J_m'(ka_1) \eta_{m,-n} \end{aligned} \tag{46}$$

in which, $\eta_{m,n}$ is just like Eq. (31). Hence, compare Eq. (45) with Eq. (46)

$$2\left[B_n^{(1)} H_n^{(1)'}(ka_1) + B_n^{(2)} H_n^{(2)'}(ka_1)\right] = \sum_{m=0}^{\infty} C_m J_m'(ka_1) \eta_{m,-n}$$

$$(n = 0, \pm 1, \pm 2, \cdots) \tag{47}$$

4.4 Displacement continuity condition on $\underline{L_1}$:

$$w^{(C)}(r,\theta) = w^{(V)}(r,\theta), \quad (r,\theta) \in \underline{L_1} \tag{48}$$

Define an auxiliary function $\Psi_2(\theta)$. When $\theta \in [0, \pi]$,

$$\begin{aligned} \Psi_2(\theta) &= \frac{1}{w_0} w^{(C)}(a_1,\theta) \\ &= \sum_{n=-\infty}^{\infty} \left[B_n^{(1)} H_n^{(1)}(ka_1) + B_n^{(2)} H_n^{(2)}(ka_1)\right] e^{in\theta} \\ &= \frac{1}{w_0} w^{(V)}(a_1,\theta) = \sum_{m=0}^{\infty} C_m J_m(ka_1) \cos m\theta \end{aligned} \tag{49}$$

It is easy to see that $\Psi_2(\theta)$ is an even function about θ in the interval $\theta \in [-\pi, \pi]$. Making $\Psi_2(\theta)$ cosine series Fourier expansion on $\theta \in [0, \pi]$:

$$\Psi_2(\theta) = \sum_{m=0}^{\infty} a_m' \cos m\theta \tag{50}$$

where

$$a_m' = (\varepsilon/\pi)\int_0^{\pi} \Psi_2(\theta) \cos\theta d\theta \ ; \quad m = 0,1,2...$$

as in Eq. (37).

Compare Eq. (49) with Eq. (50)

$$a_m' = C_m J_m(ka_1) \tag{51}$$

and

$$a_m' = \varepsilon_m \sum_{n=-\infty}^{\infty} \left[B_n^{(1)} H_n^{(1)}(ka_1) + B_n^{(2)} H_n^{(2)}(ka_1)\right] \eta_{m,n} \tag{52}$$

in which, $\eta_{m,n}$ is defined in Eq. (31). Combining Eq. (51) and Eq. (52)

$$\begin{aligned} &\varepsilon_m \sum_{n=-\infty}^{\infty} \left[B_n^{(1)} H_n^{(1)}(ka_1) + B_n^{(2)} H_n^{(2)}(ka_1)\right] \eta_{m,n} \\ &= C_m J_m(ka_1) \end{aligned}$$

$$(m = 0, 1, 2, \cdots) \tag{53}$$

The system of equations resulting from boundary conditions deduced above is Eqs. (34), (40), (47) and (53). Using Eq. (40), the set of coefficients $\{A_m\}$ can be expressed in terms of the sets $\{B_n^{(1)}\}$ and $\{B_n^{(2)}\}$. Then, $\{A_m\}$ can be eliminated after substituting the expression into Eq. (34). After a series of simplifications, Eq. (34) can be written as a function only of the unknown sets of coefficients $\{B_n^{(1)}\}$ and $\{B_n^{(2)}\}$, resulting in the following infinite system of equations:

$$\sum_{l=-\infty}^{\infty} \left[M_{nl}^{(1)}(ka) \cdot B_l^{(1)} + M_{nl}^{(2)}(ka) \cdot B_l^{(2)}\right] = m_n$$

$$(n = 0, \pm 1, \pm 2, \cdots) \tag{54}$$

in which

$$M_{nl}^{(j)}(ka) = E_{nl}^{(3)}(ka) H_l^{(j)}(ka) - H_n^{(j)'}(ka)\,\delta_{nl} \tag{55}$$

$$m_n = \frac{1}{2}\sum_{m=0}^{\infty} a_{0,m} \left[\frac{H_m^{(1)'}(ka)}{H_m^{(1)}(ka)} J_m(ka) - J_m'(ka)\right] \eta_{m,-n} \tag{56}$$

and $\delta_{nl}=0$ if $n\neq 1$ and $\delta_{nn}=1$.

$$E_{nl}^{(j)}(ka)=\sum_{m=0}^{\infty}\frac{\varepsilon_m}{2}\frac{C_m^{(j)'}(ka)}{C_m^{(j)}(ka)}\eta_{m,-n}\eta_{m,l} \tag{57}$$

with, for $j=1, 2, 3, 4$

$$C_m^{(1)}(ka)=\mathrm{J}_m(ka),\ C_m^{(2)}(ka)=\mathrm{Y}_m(ka),$$

$$C_m^{(3)}(ka)=\mathrm{H}_m^{(1)}(ka) \text{ and } C_m^{(4)}(ka)=\mathrm{H}_m^{(2)}(ka)$$

Similarly, for Eq. (46) and (52), we extract the set of coefficients $\{C_m\}$ from Eq. (52) and substitute it into Eq. (46). With $\{C_m\}$ eliminated,

$$\sum_{l=-\infty}^{\infty}\left[N_{nl}^{(1)}(ka_1)B_l^{(1)}+N_{nl}^{(2)}(ka_1)B_l^{(2)}\right]=0$$
$$(n=0,\pm1,\pm2,\cdots) \tag{58}$$

where,

$$N_{nl}^{(j)}(ka_1)=E_{nl}^{(1)}(ka_1)\cdot\mathrm{H}_l^{(j)}(ka_1)-\mathrm{H}_n^{(j)'}(ka_1)\cdot\delta_{nl} \tag{59}$$

The system of Eqs. (54) and (58) can be solved by truncating the infinite matrix into a sufficiently large finite matrix. The number of terms considered must be large enough to satisfy the required accuracy. Because of the ill-condition of the matrix, in this paper, the equations are solved using the subroutines of LAPACK (Anderson *et al.*, 1999) and using the SVD (Singular Value Decomposition) (Golub and Loan, 1996) method.

If the term $B_n^{(1)}\mathrm{H}_n^{(1)'}(ka)+B_n^{(2)}\mathrm{H}_n^{(2)'}(ka)$ is replaced by $B_n\mathrm{J}_n'(ka)$ in Eq. (34) and $B_n^{(1)}\mathrm{H}_n^{(1)}(ka)+B_n^{(2)}\mathrm{H}_n^{(2)}(ka)$ by $B_n\mathrm{J}_n(ka)$ in Eq. (40), and Eqs. (47) and (53) are eliminated, Eqs. (34) and (40) are reduced to the infinite set of linear algebraic equations for the analytical solution for the hill of a semi-circular cross-section (as the model of Yuan and Men, 1992). The numerical results show that these two solutions are equivalent.

5 Surface displacements and stress amplitudes

The dimensionless parameters used in subsequent figures are defined as follows: stress residual error on the free surface L of the hill

$$|\varepsilon(\tau)|=|\tau_{rz}^{(C)}(r,\theta)|/\tau_0 \qquad (r,\theta)\in L \tag{60}$$

and displacement and stress residual errors on the interface $\underline{L}$ and $\underline{L_1}$

$$|\varepsilon(w)|=|w^{(C)}(r,\theta)-w^{(\mathrm{ff})}(r,\theta)-w^{(\mathrm{s})}(r,\theta)|/w_0$$
$$(r,\theta)\in \underline{L} \tag{61}$$

$$|\varepsilon(\tau)|=|\tau_{rz}^{(C)}(r,\theta)-\tau_{rz}^{(\mathrm{ff})}(r,\theta)-\tau_{rz}^{(\mathrm{s})}(r,\theta)|/\tau_0$$
$$(r,\theta)\in \underline{L} \tag{62}$$

$$|\varepsilon(w)|=|w^{(C)}(r,\theta)-w^{(V)}(r,\theta)|/w_0$$
$$(r,\theta)\in \underline{L_1} \tag{63}$$

$$|\varepsilon(\tau)|=|\tau_{rz}^{(C)}(r,\theta)-\tau_{rz}^{(V)}(r,\theta)|/\tau_0$$
$$(r,\theta)\in \underline{L_1} \tag{64}$$

and the stress residual error on the wall of the tunnel L_1

$$|\varepsilon(\tau)|=|\tau_{rz}^{(C)}(r,\theta)|/\tau_0 \tag{65}$$

Since the stress residual errors on the free flat ground surface Γ and tunnel surface Γ_1 equal zero strictly by setting the wave functions, they are not discussed here.

Furthermore, the dimensionless frequency η is defined as the ratio of the width of hill $2a$ and wavelength of incident wave λ (Lee, 1988):

$$\eta=\frac{2a}{\lambda}=\frac{ka}{\pi}=\frac{\omega a}{\pi c_\beta} \tag{66}$$

Thus, the problem can be characterized in terms of the dimensionless frequency η, the radius of the tunnel to that of the hill a_1/a, and the incident angle γ.

The resulting motion will be characterized by $|w|$, the dimensionless displacement amplitudes of total motion w, and relative phases on the free surface, where

$$|w|=\left\{[\mathrm{Re}(w)]^2+[\mathrm{Im}(w)]^2\right\}^{1/2}/w_0$$
$$\mathrm{Phase}(w)=\tan^{-1}(\mathrm{Im}(w)/\mathrm{Re}(w)) \qquad (r,\theta)\in \Gamma+L \tag{67}$$

in which Re(·) and Im(·) represent the real and imaginary parts of the complex argument, respectively.

5.1 Analysis of accuracy

In order to determine the approach trend of the numerical results to the genuine solution of the problem, Figs. 3-6 demonstrate the behavior of w_b and τ_b on various boundaries for a =10.0, a_1 = 5.0, γ = 90°, different truncation order n and dimensionless frequency η (η = 0.5 and 5.0). In all figures, the longitudinal axis is characterized by logarithmic coordinates.

As seen from Figs.3-4, the errors on various boundaries do not converge synchronously. That is

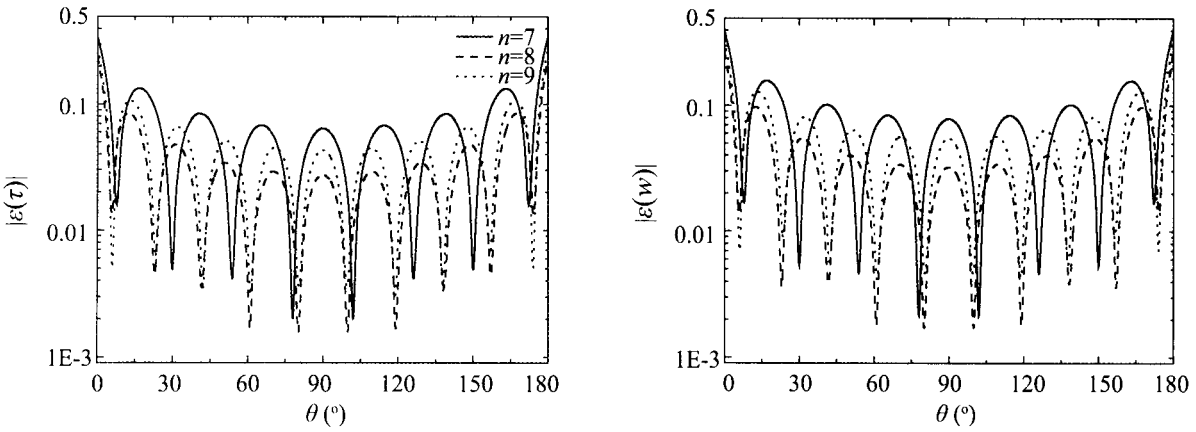

(a) Residual displacement on L_1 (b) Residual displacement on L

Fig. 3 Residual displacements on various boundaries for η = 0.5, a_1/a = 5/10, γ = 90°

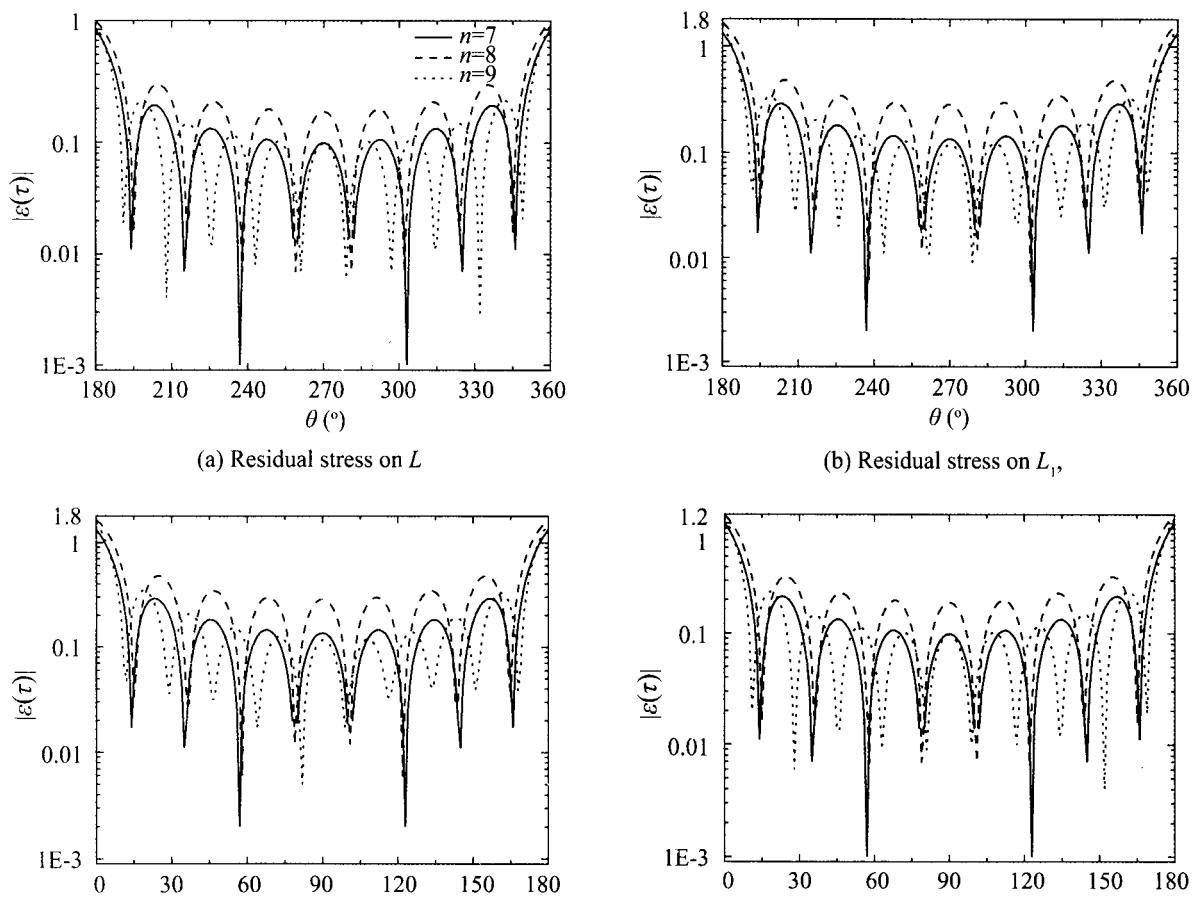

(a) Residual stress on L (b) Residual stress on L_1,

(c) Residual stress on L_1 (d) Residual stress on L

Fig. 4 Residual stresses on various boundaries for η = 0.5, a_1/a = 5/10, γ = 90°

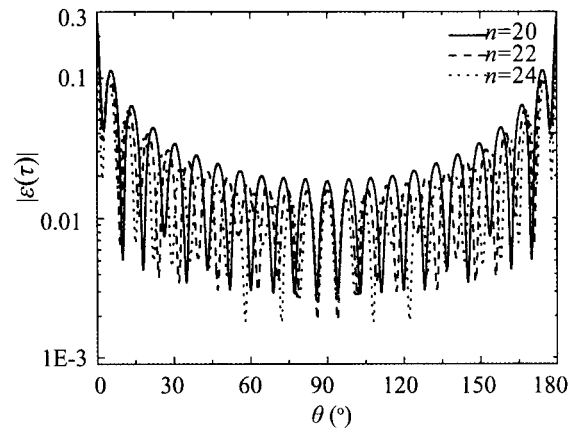

(a) Residual displacement on $\underline{L}_1$

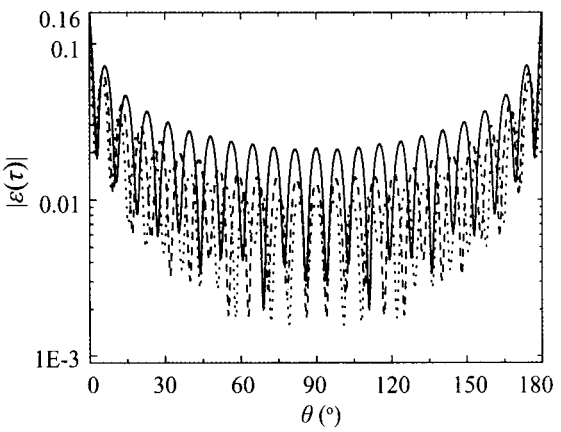

(b) Residual displacement on $\underline{L}$

Fig. 5 Residual displacements on various boundaries for $\eta = 0.5$, $a_1/a = 5/10$, $\gamma = 90^0$

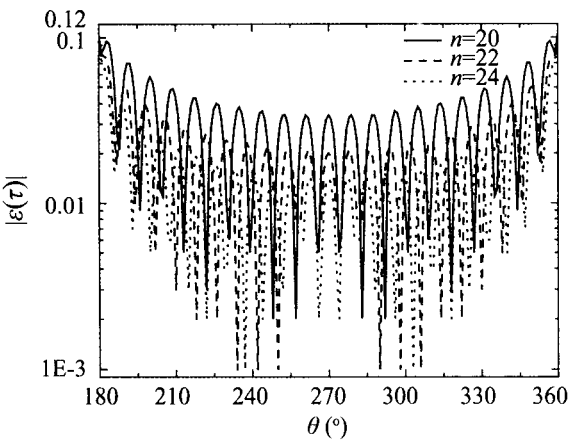

(a) Residual stress on L

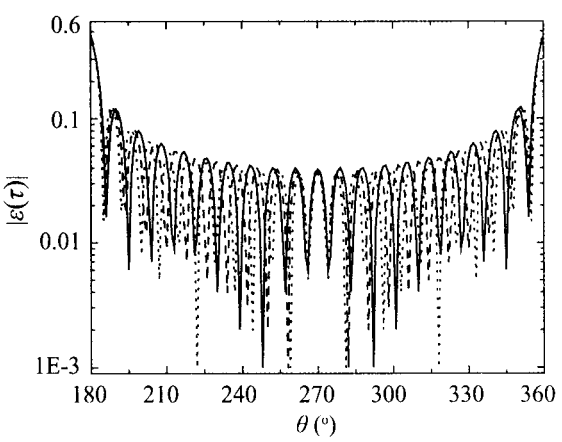

(b) Residual stress on L_1

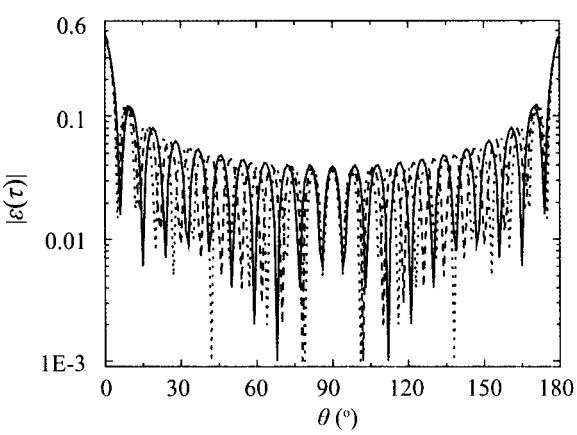

(c) Residual stress on $\underline{L}_1$

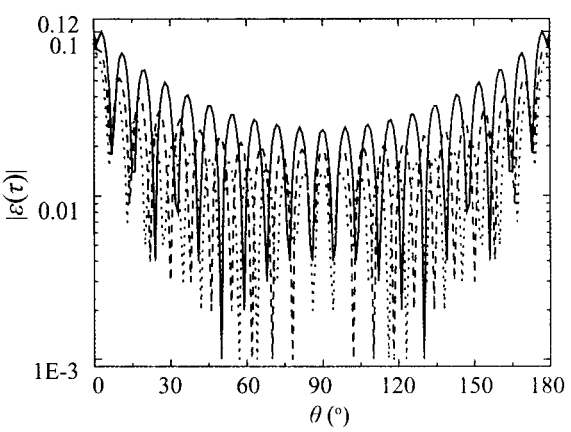

(d) Residual stress on $\underline{L}$

Fig. 6 Residual stresses on various boundaries for $\eta = 0.5$, $a_1/a = 5/10$, $\gamma = 90^0$

because there are two sets of Fourier transforms on two different circular boundaries, namely $L+\underline{L}$ and $L_1+\underline{L}_1$, and their convergent speed is not consistent. Besides, when the frequencies of incident SH waves are small, the truncation orders are also small. For instance, in Figs 3, 4 and 5, 6, the truncation orders are 10 and 29, respectively. Thus, both of these Fourier expansions may not converge together at the same truncation order. Figures 5-6 show that the displacement and stress errors approach zero with an increasing truncation order when the frequency of the incident wave grows larger. In fact, there is a similar phenomenon that appears when

the radius ratio a_1/a is too small or large. Therefore, in this analysis, only moderate cases are discussed for the purpose of ensuring the accuracy of the numerical results.

It can be seen from the above figures that the residual stresses at the outer rims and tunnel inner rims of the hill remain at a relatively high value even with the truncation order n increase. One possible reason is that, as stated by Yuan and Liao (1996), the hill outer rims and tunnel inner rims are possibly singular points for stress. Further, the stress auxiliary functions $\Phi_1(\theta)$ and $\Phi_2(\theta)$ adopted from Yuan and Liao (1996) that were used here are discontinuous at the rims; namely, at the points of $\theta=0,\pi$ the stress functions have 'jumps', from nonzero to zero values on the hill top. Expansion of discontinuous functions in terms of Fourier series will lead to Gibb's phenomena, namely overshooting at points of discontinuity of $\Phi_1(\theta)$ and $\Phi_2(\theta)$. Therefore, the stresses as well as displacements at the four rims are not accurate in this paper. However, Figs. 3-6 indicate that on average, all residuals converge to zero on the entire boundary of auxiliary functions. This means that with Fourier series expansion, the effect of hill and tunnel rims on the accuracy of the solution is limited only in the very small region near the hill and tunnel rims. The authors believe that reducing this discrepancy will require a new formulation and methods to solve this problem, without using the stress and displacement functions $\Phi_1(\theta)$ and $\Phi_2(\theta)$ at the circular interface between the hill and half space. Further research on this subject is a high priority for the authors.

5.2 Three dimensional figures

Figures 7 and 8 show the surface displacement amplitudes, plotted versus the dimensionless distance x/a and the dimensionless frequency, η, for angles of

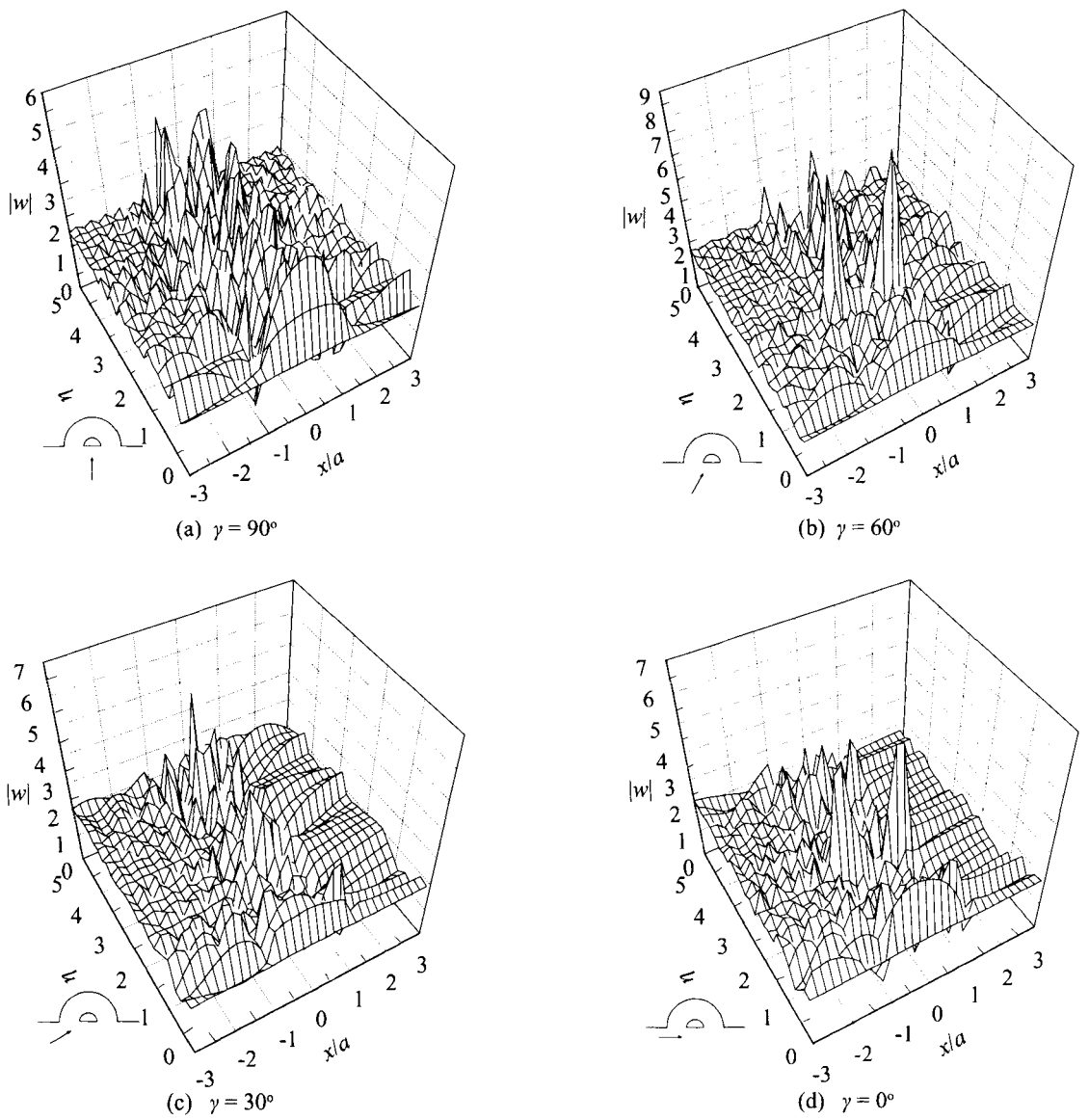

Fig. 7 Displacement amplitudes versus dimensionless frequency: a_1/a = 5/10

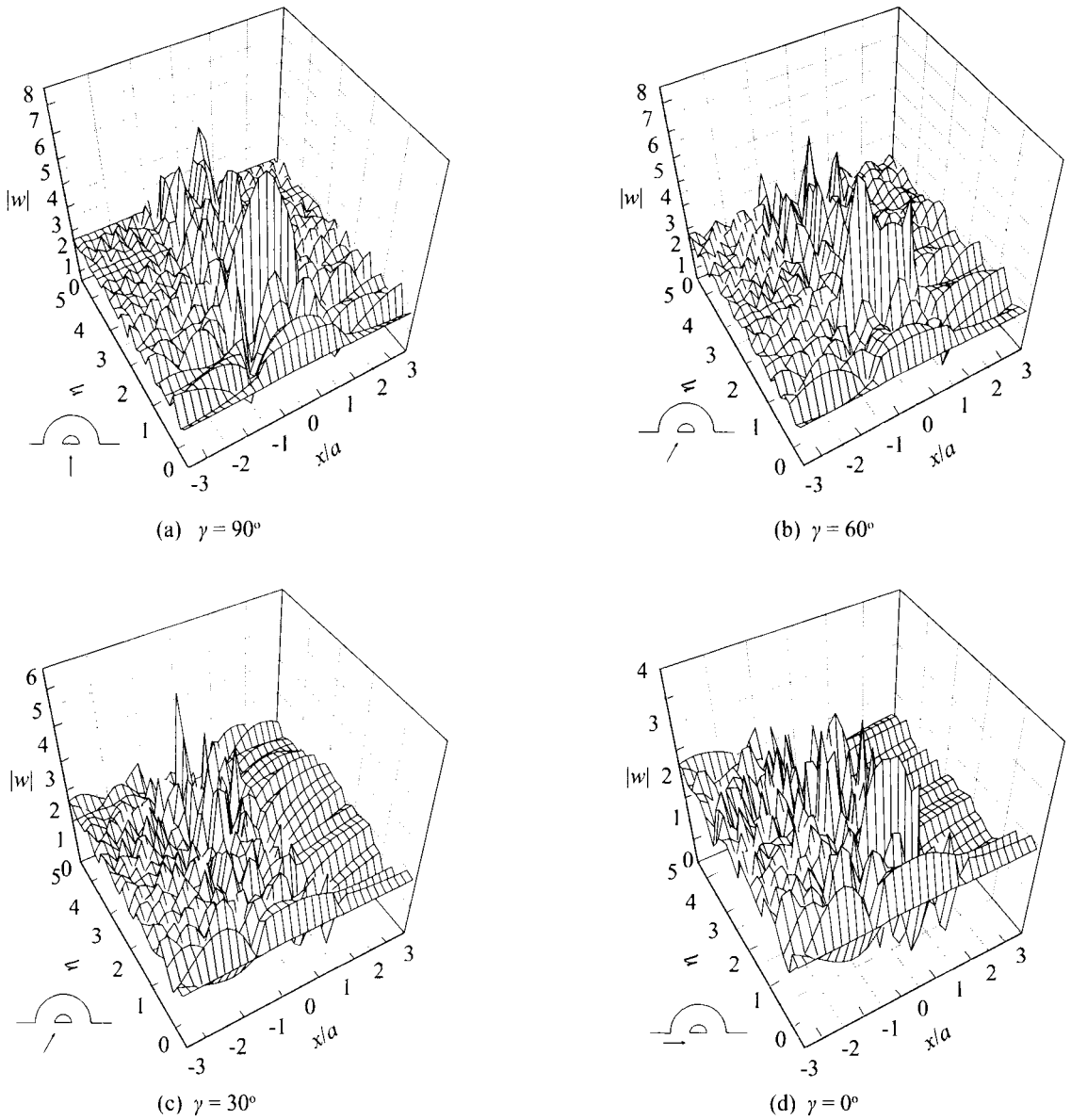

(a) $\gamma = 90^{\circ}$ (b) $\gamma = 60^{\circ}$

(c) $\gamma = 30^{\circ}$ (d) $\gamma = 0^{\circ}$

Fig. 8 Displacement amplitudes versus dimensionless frequency: a_1/a = 3/10

incidence γ = 90° (vertical) and 0° (horizontal) and corresponding to the radius ratio of tunnel and hill as a_1/a=5/10 and 3/10. In these figures, the displacement amplitudes on the surface of the hill are plotted along the axis x/a in the interval $-1 \le x/a \le 1$. The point x/a=−1 corresponds to the left rim of the hill, x/a=0 to the top and x/a =1 to the right rim. The incident SH waves are assumed to arrive from the left (x/a<0) in all cases except that of vertical incidence (γ = 90°). It can be seen from the four figures that the complexity of the surface displacements increases with increasing frequency η. For horizontal incidence (γ = 0°), the complexity of the surface displacement amplitudes increases on the side of the half space facing the incoming waves ($x/a < -1$), and becomes relatively smoother on the other side ($x/a > 1$). The zone behind the surface (canyon, valley or hill) and subsurface (cavity or inclusion) topographies is often referred to as the shadow zone.

The maximum amplitudes as high as 8.5 around when $\eta \approx 2.2$ are observed near the left rim of the hill in Fig. 7 (b). Liang *et al.* (2004), in studying diffraction of SH waves by a hill with a concentric circular tunnel, made similar observations. However, in the study of diffraction of SH waves by a hill without tunnel (Yuan and Liao, 1996), the displacement amplitudes only reach 3.9. These phenomena may be explained by the fact that, some diffracted waves are more easily reflected repeatedly between the surfaces of the hill and the top of the tunnel, resulting in a standing wave pattern (similar to an echo). This mechanism of wave motion is similar to the diffraction of SH waves by a canyon above a subsurface tunnel (Lee *et al.*, 1999). At low frequencies (e.g., less than 0.05), the graph shows that every point on the half-space surface and the hill has displacement amplitudes close to 2.0; however, as frequencies slightly increase (e.g., larger than 0.1), the displacement

amplitudes in the hills can greatly increase as a result of diffraction.

5.3 Two dimentional results of the ground surface displacements

Figures 9-12 show the effects of the incident angle and dimension of the tunnel on the ground surface displacements. The calculated parameters are: ratio of tunnel and hill a_1/a = 3/10 and 5/10, dimensionless frequency η = 3.0 and 5.0, and four different incident angles of 90°, 60°, 30° and 0°.

From viewing the figures below, we see that the incident angles of SH waves and the tunnel's dimension can both affect the pattern of the surface displacements. If there is no tunnel, a shadow zone is observed behind the canyon by horizontal incident SH waves (Yuan and Liao, 1996). The same phenomena is seen in the following figures. The displacement amplitudes behind the hill for horizontal incident SH waves are always lower than those of the free field and in front of the hill. The same observations have also previously been made for the case of SH waves incident on a canyon (Cao and Lee, 1989) and underground cavity (Lee, 1977). In Figs. 10 and 12, vertical incidence cases, ground motion is concentrated in the hill region (i.e., $x/a \in [-1,1]$). The frequencies of incident SH wave are

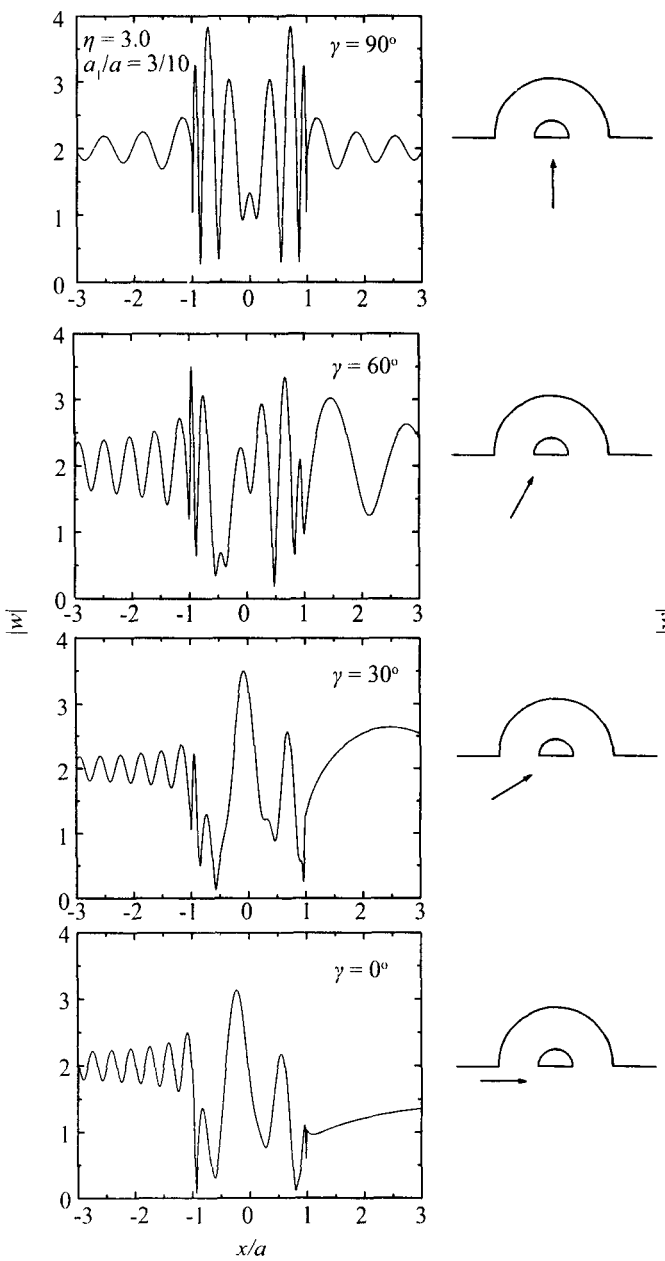

Fig. 9 Surface displacement amplitudes at four angles of incidence: η = 3.0, a_1/a = 3/10

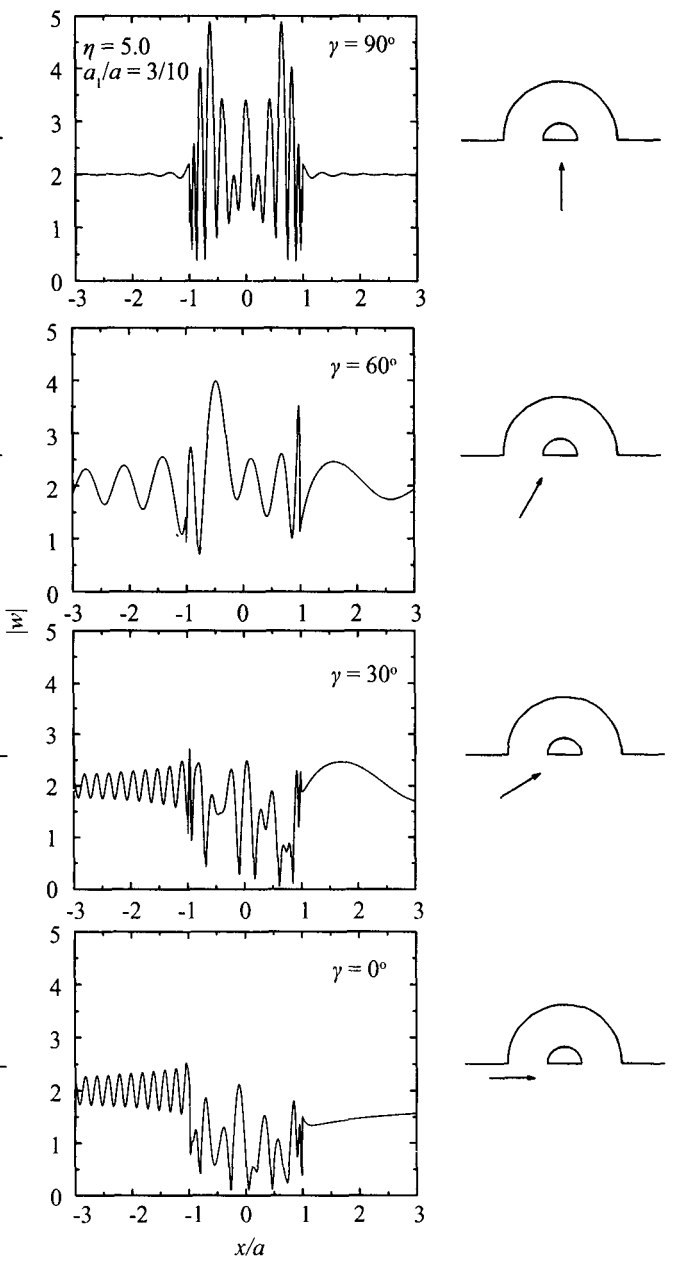

Fig. 10 Surface displacement amplitudes at four angles of incidence: η = 5.0, a_1/a = 3/10

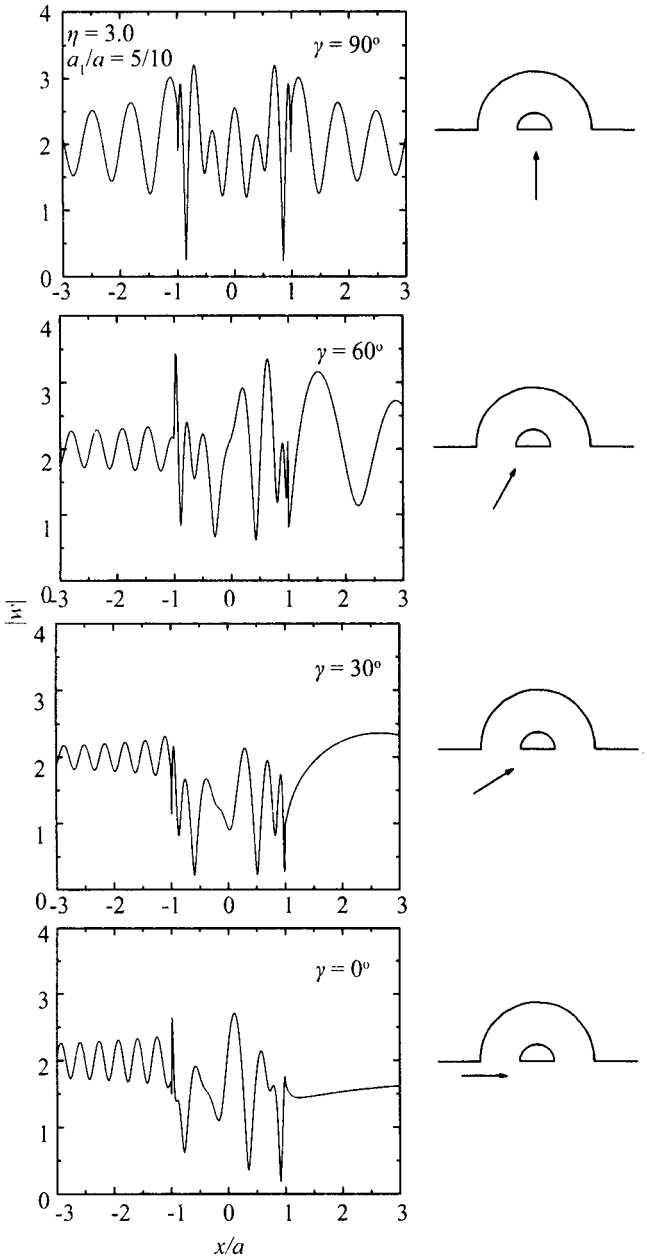

Fig. 11 Surface displacement amplitudes at four angles of incidence: $\eta = 3.0$, $a_1/a = 5/10$

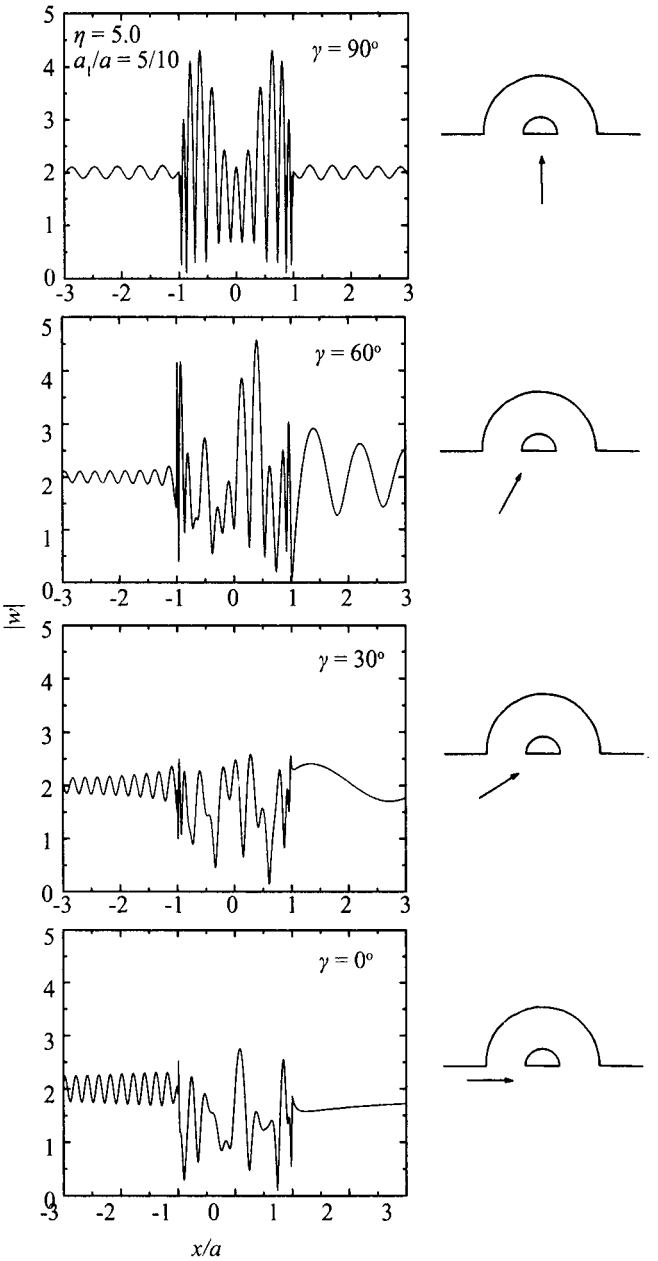

Fig. 12 Surface displacement amplitudes at four angles of incidence: $\eta = 5.0$, $a_1/a = 5/10$

close to certain natural vibration frequencies of the hill-tunnel system, which cause resonances to occur in these two cases.

6 Conclusions

An analytical solution for scattering of incident SH waves by a semi-cylindrical hill with a concentric semi-cylindrical tunnel was derived by wave function expansion and the auxiliary function technique. Complex exponential and cosine forms of Fourier expansion theorem are used. This method may be applied to further studies involving mixed boundary problems. Observations are as follows:

(1) The amplification of surface displacement amplitudes at some points around a hill can be as high as two times the free-field motions.

(2) The utilization of complex exponential and cosine forms of Fourier expansion theorem can improve the efficiency and precision of mixed boundary problems. However, the range of resoluble cases is still limited by Gibb's phenomena, the complexity of the model, and the precision of the variables of computer language.

(3) The incident angles of SH waves and the dimension of the tunnel can both affect the pattern of the surface displacements. In hills with no tunnels, a shadow zone is observed behind the canyon.

(4) The dimensionless frequency η plays an important role in determining the displacement patterns. Larger values of η will result in more complex displacements and higher amplifications.

References

Abramowitz M and Stegun IA (1972), *Handbook of Mathematical Functions, with Formulas, Graphs, and Mathematical Tables*, Dover Publications, Inc., New York, N.Y.

Anderson E, Bai Z, Bischof C, Blackford S, Demmel J, Dongarra J, DuCroz J, Greenbaum A, Hammarling S, McKenney A and Sorensen D (1999), *LAPACK User's Guide*. 3rd ed., SIAM Publications, Philadelphia. (http://www.netlib.org/lapack/lug/lapack_lug.html)

Cao H and Lee VW (1989), "Scattering of Plane SH Waves by Circular Cylindrical Canyons with Variable Depth-to-width Ratio," *European Journal of Earthquake Engineering*, **3**(2): 29-37.

Golub Gene H and Charles F Van Loan (1996), *Matrix Computations*, 3rd ed., Johns Hopkins University Press, Baltimore, Maryland.

Lee VW (1977), "On Deformations Near Circular Underground Cavity Subjected to Incident Plane SH Waves," *Proceedings of the Application of Computer Methods in Engineering Conference*, Univ. of Southern California, Los Angeles, CA, Vol.II, pp. 951-962.

Lee VW and Chen S (1998), "Deformations Near Surface and Subsurface (Multiple Foundations Above Subway Tunnel) Topographies," *Proc., 1st China-USA-Japan Workshop on Civil Infrastruct. Sys.*, Nov. 4-6, Shanghai, China.

Lee VW, Chen S and Hsu IR (1999), "Antiplane Diffraction from Canyon Above Subsurface Unlined Tunnel," *Journal of Engineering Mechanics*, ASCE, **125**(6): 668-675.

Lee VW and Trifuanc MD (1979), "Response of Tunnels to Incident SH-waves," *Journal of the Engineering Mechanics Division*, ASCE, **105**: 643-659.

Liang JW, Luo H and Lee VW (2004), "Scattering of Plane SH Waves by a Circular-arc Hill with a Circular Tunnel," *ACTA Seismologica Sinica*, **17**(5): 549-563.

Pao YH and Mow CC (1973), *Diffraction of Elastic Waves and Dynamics Stress Concentrations*, Crane, Russak & Company Inc., New York, N.Y.

Trifunac MD (1971), "Surface Motion of a Semi-Cylindrical Alluvial Valley for Incident Plane SH Wave," *Bulletin of Seismological and Society of America*, **61**: 1755-1770.

Trifunac MD (1973), "Scattering of Plane SH Wave by a Semi-cylindrical Canyon." *Earthquake Engineering and Structural Dynamics*, **1**: 267-281.

Wong HL and Trifunac MD (1974), "Surface Motion of a Semi-elliptical Alluvial Valley for Incident Plane SH Waves", *Bulletin of the Seismological Society of America*, **64**: 1389-1408.

Yuan XM and Liao ZP (1996), "Surface Motion of a Cylindrical Hill of Circular-arc Cross-section for Incident Plane SH Waves," *Soil Dynamics and Earthquake Engineering*, **15**: 189-199.

Yuan XM and Men FL (1992), "Scattering of Plane SH Waves by a Semi-cylindrical Hill," *Earthquake Engineering and Structural Dynamics*, **21**: 1091-1098.